

**Can differences in the nickel abundance in Chandrasekhar mass
models explain the relation between brightness and decline rate of
normal Type Ia Supernovae?**

Paolo A. Mazzali^{1,3}, Ken'ichi Nomoto^{2,3}, Enrico Cappellaro⁴,
Takayoshi Nakamura², Hideyuki Umeda², Koichi Iwamoto⁵

Received _____; accepted _____

¹Osservatorio Astronomico, Via Tiepolo, 11, Trieste, Italy

²Department of Astronomy, School of Science, University of Tokyo, Tokyo, Japan

³Research Center for the Early Universe, School of Science, University of Tokyo, Tokyo,
Japan

⁴Osservatorio Astronomico, vicolo dell'Osservatorio, 5, Padova, Italy

⁵Department of Physics, College of Science and Technology, Nihon University, Tokyo,
Japan

ABSTRACT

The use of Type Ia supernovae as distance indicators relies on the determination of their brightness. This is not constant, but it can be calibrated using an observed relation between the brightness and the properties of the optical light curve (decline rate, width, shape), which indicates that brighter SNe have broader, slower light curves. However, the physical basis for this relation is not yet fully understood. Among possible causes are different masses of the progenitor white dwarfs or different opacities in Chandrasekhar-mass explosions. We parametrise the Chandrasekhar-mass models presented by Iwamoto et al. (1999), which synthesize different amounts of ^{56}Ni , and compute bolometric light curves and spectra at various epochs. Since opacity in SNe Ia is due mostly to spectral lines, it should depend on the mass of Fe-peak elements synthesized in the explosion, and on the temperature in the ejecta. Bolometric light curves computed using these prescriptions for the optical opacity reproduce the relation between brightness and decline rate. Furthermore, when spectra are calculated, the change in colour between maximum and two weeks later allows the observed relation between $M_B(\text{Max})$ and $\Delta m_{15}(B)$ to be reproduced quite nicely. Spectra computed at various epochs compare well with corresponding spectra of spectroscopically normal SNe Ia selected to cover a similar range of $\Delta m_{15}(B)$ values.

1. Introduction

The use of Type Ia Supernovae (SNe Ia) to probe cosmological parameters relies on the possibility to calibrate the absolute magnitude of individual SNe from the observed luminosity evolution (for a review see, e.g. , Branch 1998). Pskovskii (1977) first suggested that brighter SNe Ia decline more slowly than dimmer ones. This was later confirmed by Phillips (1993). Using modern data for a small sample of well observed local SNe Ia he showed that the relation exists in the B , V and I bands, but it is steepest in B . The relation between maximum B brightness and the number of magnitudes the B band declines in the first 15 days after maximum, a quantity called $\Delta m_{15}(B)$, is commonly referred to as the Phillips’ relation. Hamuy et al. (1995, 1996b) confirmed the relation using a bigger sample of objects, although their slopes were flatter than Phillips’ original values.

Riess et al. (1995) used a more sophisticated approach based on the analysis of the entire early light curve, which allows the SN maximum brightness to be determined by comparison with a set of template light curves of objects whose distance and reddening are assumed to be known. However, the absolute magnitude - light curve shape relation is not yet calibrated exactly, as is shown by the differences among recent work (Riess et al. 1995, 1998).

Although the relation between SN Ia brightness and decline rate has been used extensively, its physical bases are not yet understood. Several groups have published synthetic light curves obtained from explosion models which differ in many of their properties (progenitor WD mass, mode of the explosion). These light curves span a wide range of maximum brightness and decline rates, and although there are models that appear to reproduce some of the observations, a fully consistent picture is still lacking. In this paper we explore the possibility that a series of Chandrasekhar-mass explosion models, which differ essentially in the amount of ^{56}Ni they synthesize, can explain the observed

range of light curves and spectra of at least *spectroscopically normal* SNe Ia.

2. Basic Light Curve Physics

SNe Ia synthesize significant amounts of radioactive ^{56}Ni , and their light curves are powered by the deposition in the expanding SN ejecta of the γ -rays and positrons produced by the decay chain $^{56}\text{Ni} \rightarrow ^{56}\text{Co} \rightarrow ^{56}\text{Fe}$.

The shape of the light curve of a SN Ia near maximum depends essentially on the fact that optical photons emitted upon the deposition and thermalization of the γ -rays and positrons do not immediately escape from the SN. These photons must in fact first propagate through the optically thick SN ejecta, where they interact with spectral lines and free electrons until they are redshifted into a region of the spectrum where the opacity is low and they can escape. Since the opacity is dominated by line processes, these regions correspond to wavelengths where line opacity is low. This gives rise to the very characteristic SN Ia spectrum, with broad absorption features and few P-Cygni emissions, which correspond to these 'opacity windows' (e.g. Pinto & Eastman 2000, Mazzali 2000).

Since it takes photons a finite time to emerge from the ejecta in what is essentially a random walk process, very soon after the explosion the SN luminosity is lower than the energy input into the ejecta. Maximum light occurs when the instantaneous rates of deposition of hard radiation and emission of optical light are roughly equal (Arnett 1982). As time goes on, the delay between energy deposition and emission of optical radiation becomes smaller and smaller. At late times, in the so-called nebular phase, γ -ray deposition becomes less efficient, and a significant contribution to the light curve is made by the positrons, which are supposed to deposit *in situ* if a weak magnetic field is present in the ejecta. Positrons carry only about 3.5% of the total decay energy.

The properties of the peak of a SN Ia light curve have been studied analytically by Arnett (1982, 1996). The basic features are:

1. The brightness of the light curve at maximum is proportional to the mass of synthesized ^{56}Ni .
2. The width of the light curve τ_{LC} depends on the ejected mass, the kinetic energy of the explosion and the optical opacity as follows:

$$\tau_{\text{LC}} \propto \kappa_{\text{opt}}^{1/2} M_{\text{ej}}^{3/4} E_{\text{K}}^{-1/4}. \quad (1)$$

Here M_{ej} is the ejected mass (i.e. the WD mass, since SNe Ia are not supposed to leave a remnant behind), E_{K} is the kinetic energy of explosion and κ_{opt} is the grey opacity to optical photons.

3. Observational facts and interpretation

That SNe Ia do indeed synthesize different amounts of ^{56}Ni is an established observational fact. Spectroscopically ‘normal’ SNe Ia produce roughly $0.5 M_{\odot}$, but extreme cases range from $0.1 M_{\odot}$ for SN 1991bg (Filippenko et al. 1992) to about $1 M_{\odot}$ for SN 1991T (Spyromilio et al. 1992). These extreme cases are spectroscopically peculiar SNe. However, even among ‘normal’ SNe Ia a distribution of properties is observed (Nugent et al. 1995, Fisher et al. 1995), which is quite likely the result of different synthesized ^{56}Ni masses (Mazzali et al. 1998, Contardo et al. 2000). Can these differences in the mass of ^{56}Ni influence not only the peak brightness, but also the width of the light curves?

One possibility is to assume that all SNe Ia are self-similar events, but that the progenitor masses, hence M_{ej} , are different, so that all other parameters (^{56}Ni mass, E_{K}) scale accordingly. This could explain the observations in a rather straightforward

manner. However, this interpretation implies that sub-Chandrasekhar events, and possibly super-Chandrasekhar ones (e.g. SN 1991T, Fisher et al. 1999) are very common, since such events would be necessary to explain not only spectroscopically peculiar events, but also the faint end of the ‘normal’ SN Ia sequence (see e.g. Cappellaro et al. 1997). This is currently not a favourite scenario among the ‘explosive’ community, since sub-Chandrasekhar explosions that have the correct element distribution are difficult to design (e.g., Hillebrandt & Niemeyer 2000).

Another possibility is a change of E_K only. However, E_K is produced in almost equal amounts by burning a given mass to NSE (i.e. mostly to ^{56}Ni), or by incomplete burning to Intermediate Mass Elements (IME) such as Si and S. Therefore, one can expect that those SNe which synthesize more ^{56}Ni are not likely to have a much higher E_K than SNe which produce less ^{56}Ni , unless the total mass burned (to NSE or to IME’s) is also larger. Since in most models the WD is almost completely burned to either ^{56}Ni or to IME’s, (~ 1.2 – $1.3 M_\odot$ for a Chandrasekhar mass white dwarf, Nomoto et al. 1984, 1994, Woosley & Weaver 1994) there is not much room for a large E_K variation if the mass of the progenitor WD is constant. Also, the width of the light curve depends only weakly on E_K .

So, if we want to restrict ourselves to Chandrasekhar-mass explosions, a variation in the opacity κ_{opt} is the most promising direction to follow.

Many models exist of Chandrasekhar-mass explosions. Models differing in the details of burning and flame propagation can produce different amounts of ^{56}Ni (usually in the range $0.4 - 0.8 M_\odot$) and display different light curves (see, e.g., Höflich et al. 1995, 1998 and references therein). Different masses of ^{56}Ni lead naturally to different SN brightnesses.

Among the possible physical reasons that could make a SN Ia explosion synthesize different amounts of ^{56}Ni are a different value of the deflagration speed (caused by a different buoyancy force) or of the density at which the burning wave makes a transition

from a deflagration to a detonation (DDT). Umeda et al. (1999) suggested that a different C/O ratio in the progenitor WD may cause a variation in the deflagration speed or in the deflagration-to-detonation transition density ρ_{DDT} .

Iwamoto et al. (1999, see also Brachwitz et al. 2000) computed the explosion hydrodynamics and the nucleosynthesis for three representative cases of ρ_{DDT} . In their models, the explosion starts as a slow deflagration, leading to the synthesis of a small amount ($\sim 0.1 M_{\odot}$) of Fe-group isotopes (^{54}Fe , ^{56}Fe , ^{58}Fe , ^{58}Ni). The exact ratios of these isotopes depend on the value of the electron fraction Y_e , which in turn depends on the central density and composition of the WD and on the flame speed. Meanwhile the WD expands, electron capture decreases and as the burning proceeds further out radioactive ^{56}Ni is mostly synthesized. Eventually, the deflagration enters the region of incomplete Si burning and explosive O burning, where the transition to a detonation occurs. In the detonated region, both ^{56}Ni and IME's are produced. The amount of ^{56}Ni produced in the detonated layer (after DDT) is sensitive to ρ_{DDT} . For a higher value of ρ_{DDT} , the detonated regions reach higher temperatures because of smaller specific heats, and so more ^{56}Ni is produced and the SN Ia is brighter. The WS15 series of models: DD1, DD2 and DD3 of Iwamoto et al. (1999) synthesize 0.56, 0.69 and 0.77 M_{\odot} of ^{56}Ni , respectively, for values of ρ_{DDT} ranging from 1.7 to 3.0 10^7g cm^{-3} . The three models WS15 have the same slow deflagration speed (1.5% of the sound speed), thus the amount of ^{56}Ni synthesized in the deflagration zone is the same and the difference in the masses of ^{56}Ni synthesized is due entirely to the different ρ_{DDT} .

An interesting property of the models presented by Iwamoto et al. (1999) is that the total mass of Fe-peak elements (mostly ^{56}Ni) plus IME's is roughly constant ($\approx 1.28 - 1.30 M_{\odot}$), so that all models also have about the same E_K ($1.33 - 1.43 10^{51} \text{erg}$). Note that such a small range of E_K would introduce a change of only less than 2% in τ_{LC} . It is therefore

safe to ignore these differences. Therefore both E_K and M_{ej} are eliminated from Eq.(1) and only the dependence of τ_{LC} on κ_{opt} remains. This feature makes these models particularly appealing for an investigation of their photometric and spectroscopic properties. The idea is to verify whether such a spread in the properties of the models can explain the observed spread of properties of at least *spectroscopically normal* SNe Ia.

The question is how can a different $^{56}\text{Ni}/\text{IME}$ ratio affect κ_{opt} . There seem to be two ways that this can happen. One is that more ^{56}Ni leads to more heating and therefore to a larger κ_{opt} (Khokhlov et al. 1993, Höflich et al. 1996). However, since most of the ^{56}Ni is not mixed, an increase in the total production of ^{56}Ni does not immediately translate into a higher temperature. The other possibility stems from the consideration that the opacity in the ejecta of a SN Ia is dominated by line opacity of low ionization species. Pauldrach et al. (1995) showed that the $\tau_e = 1$ surface in W7-type ejecta at an epoch of 25 days falls at $v \sim 5000 \text{ km s}^{-1}$, which is significantly less than the photospheric velocity at that epoch. In the conditions that apply in a SN Ia near maximum, the time a photon spends scattering in lines as it redshifts its way out of the expanding envelope is much shorter than the time spent travelling from one line to the next redder line (Pinto & Eastman 2000, Mazzali 2000). The crossing of each line in frequency space can thus be treated as a single scattering event, so that the opacity depends simply on the number of active lines, which in turn depends on which elements dominate the composition. In particular, low excitation ions of Fe-group elements (Fe I–Fe III, Co I–Co III, Ni I–Ni III etc.) have many more lines (about a factor of 10) than low excitation ions of IME’s (Si I–Si II, S I–S II, Ca I–Ca II etc.). It may therefore not be unreasonable to expect that the average opacity is higher in regions where the abundance of the Fe-group elements is higher. On average, one can therefore expect that SNe with a higher $^{56}\text{Ni}/\text{IME}$ production ratio also have a higher opacity.

4. Explosion models

Since our aim was to test one basic aspect of the light curve, namely the dependence on the composition of the ejecta, we chose to simplify the input as much as possible. In particular, since the models published by Iwamoto et al. (1999) have similar density distributions (because they have similar E_K , $\sim 1.3 - 1.4 \cdot 10^{51}$ erg), we adopted the W7 (Nomoto et al. 1984) distribution as an average for all models. This is a reasonable approximation because $\rho(v)$ does not change greatly among different Chandrasekhar-mass explosion models, and W7 is a good representation of the typical $\rho(v)$. However, if the mass of ^{56}Ni translates more or less directly into luminosity at maximum, the spread in ^{56}Ni mass of the Iwamoto et al. (1999) models corresponds to a spread of maximum brightness of only about 0.35 mag. This is less than the observed spread of ‘normal’ SNe Ia (~ 0.6 mag). Therefore, we constructed models which produce 0.4, 0.6 and 0.8 M_\odot of ^{56}Ni , respectively, corresponding to $\rho_{\text{DDT}} = 1.3 - 3 \cdot 10^7 \text{g cm}^{-3}$ (Iwamoto et al. 1999; Umeda et al. 1999).

In order to do this we followed the properties of the WS15 DD series of models by Iwamoto et al. (1999). In these models, ^{56}Ni is synthesized outside of an enclosed mass of $\sim 0.1 M_\odot$, and it is the dominant element in the ejecta until the IME region is reached. Models with different masses of ^{56}Ni are therefore characterized by a different outer extent of the ^{56}Ni -dominated shell. Therefore we placed the interface between the ^{56}Ni and the IME-dominated regions at the mass coordinate appropriate to reach the required value of the ^{56}Ni mass. The abundance distribution of our parametrised models is shown in Fig.1. Using only two main contributions to the opacity, i.e. binning all elements into either Fe-group or IME, is also a step towards simplifying the models, and it is justified because none of the lighter ions have such a complicated level structure as any of the dominant Fe-group ions. It should be noticed that the distribution of ^{56}Ni in velocity space in the simple models we constructed compares favourably with the velocity of the ^{56}Ni sphere

derived by Mazzali et al. (1998) when fitting the width of the Fe II] and Fe III] emission lines in normal SNe Ia at late times.

5. Calculations

In order to test the properties of these explosion models we adopt a 2-step approach. First we compute the *bolometric* light curves using a Monte Carlo code (Cappellaro et al. 1997). Our input models consist of a density-velocity distribution, and three basic contributions to the composition are singled out. In fact, for each of the shells into which the ejecta are divided in our calculation we input the initial ^{56}Ni abundance, $X_{^{56}\text{Ni}}$, according to which γ -rays are injected in the appropriate shell following the decay law, and the total abundance of the Fe-group elements, $X_{\text{Fe-gp}}$, which includes ^{56}Ni and its daughter nuclei but also stable isotopes such as ^{54}Fe , ^{56}Fe , and ^{58}Ni . These contribute to the opacity but are not sources of γ -rays. The remaining fraction of a shell’s mass is attributed to IME’s.

As a first approximation, we initially adopted a formula for κ_{opt} which depends only on the relative abundance of Fe-group and IME. Since on average the number of active lines in an Fe-group is about 10 times larger than in an IME ion, we define the optical opacity as:

$$\kappa_{\text{opt}} = 0.25X_{\text{Fe-gp}} + 0.025(1 - X_{\text{Fe-gp}}) \quad [\text{cm}^2\text{g}^{-1}]. \quad (2)$$

The opacity is assigned a value in each of the shells into which the ejecta have been divided. With this formula, κ_{opt} ranges from $0.25 \text{ cm}^2 \text{ g}^{-1}$ in regions where Fe-group dominates to $0.025 \text{ cm}^2 \text{ g}^{-1}$ in regions where Fe-group is absent, and has a value $0.1375 \text{ cm}^2 \text{ g}^{-1}$ if the composition is 50% Fe-group and 50% IME. This is a reasonable representation of the value of κ_{opt} (see Khokhlov et al. 1993, Figure 24). However, the bolometric light curves computed with this formulation of the opacity peak too soon ($\approx 15 - 16$ days) and drop too rapidly: $\Delta m(15)(\text{Bol})$ for these light curves ranges from 0.75 mag for model Ni08 to 0.85

mag for model Ni04. Typical risetimes of local SNe Ia are about 19–20 days (Riess et al. 1999), and values of $\Delta m(15)(Bol)$ for normal SNe Ia range from 0.9 to 1.2 mag (Contardo et al. 2000).

The early rise and the slow decline of these synthetic light curves suggests that the opacity is underestimated before maximum and overestimated after maximum. Khokhlov et al. (1993) pointed out that the temperature has also a significant influence on the opacity, which is rapidly reduced as the temperature drops below 10^4 K, which is the effective temperature of observed normal SNe Ia around maximum. We therefore added a time-dependent term to the opacity equation to mimic the decrease of temperature, and hence of opacity, with time. We adopted the formula:

$$\kappa_{\text{opt}} = [0.25X_{\text{Fe-gp}} + 0.025(1 - X_{\text{Fe-gp}})] \left(\frac{t_d}{17}\right)^{-\frac{3}{2}} [\text{cm}^2\text{g}^{-1}], \quad (3)$$

but we limited the time-dependent term on the right to a maximum value of 2. With this formulation, the value of κ_{opt} for a region where both Fe-group and IME have an abundance of 0.5 is $0.275 \text{ cm}^2 \text{ g}^{-1}$ at 10 days and earlier, $0.137 \text{ cm}^2 \text{ g}^{-1}$ at 17 days and only $0.06 \text{ cm}^2 \text{ g}^{-1}$ at 30 days. This increased pre-maximum value should reflect both the higher temperature and density at those epochs and the greater relevance of the electron scattering opacity.

The basic properties of the synthetic bolometric light curves computed with this formulation of the opacity are summarized in Table 1. As expected, models which produce more ^{56}Ni are brighter and decline more slowly. In Figure 2 the synthetic light curves are compared to the *uvoir* light curves of 3 spectroscopically normal SNe which have different values of $\Delta m_B(15)$: SN 1990N ($\Delta m_B(15) = 1.07$ mag); SN 1994D ($\Delta m_B(15) = 1.31$ mag) and SN 1992A ($\Delta m_B(15) = 1.47$ mag). The observed *uvoir* light curves have been shifted along the y-axis to obtain a best overall match to the synthetic light curves, which are not meant to be detailed fits of these SNe. The *uvoir* light curve of SN 1990N was computed

using the Cepheid distance modulus $m - M = 32.03$ mag (Saha et al. 1997) and shifted upwards by 0.1 mag. The light curve of SN 1992A was taken from Suntzeff (1996), who used an SBF distance modulus $m - M = 30.65$ mag, and shifted upwards by 0.8 mag, resulting in a distance modulus $m - M = 31.45$ mag, which is consistent with the GCLF distance $m - M = 31.35$ mag published by Della Valle et al. (1998). Both of these SNe are therefore compatible with the ‘long’ distance scale. Finally, the light curve of SN 1994D was computed using the recently published GCLF distance modulus $m - M = 30.40$ mag (Drenkhahn & Richtler 1999). However, this light curve had to be shifted upwards by as much as 0.75 mag to match the light curve of model Ni06, so that the distance used for the plot in Figure 2 is $m - M = 31.15$ mag. Although this appears to be inconsistent with the GCLF distance, we note that SN 1994D had an SBF distance modulus $m - M = 30.86$ mag (Hamuy et al. 1996a). Typically, GCLF distance are larger than SBF ones, so the distance we have used for Figure 2 may not be inconsistent with the ‘long’ distance scale. Also, $\Delta m_B(15)$ of model Ni06 matches very closely the same quantity for SN 1994D (see Table 2).

Although the synthetic bolometric light curves match the *uvoir* ones reasonably well, the decline of the bolometric light curves in the 15 days following maximum is smaller than the observed B -band decline. However, the observed B -band decline is faster than the observed V -band decline, and the observed SN Ia colour changes from $B - V \sim 0$ at maximum to $B - V \sim 0.6$ at two weeks after maximum, so the fast decline of the B magnitude must be at least partially the result of a change towards the red of the colour of the spectrum. Note that all light curves reach maximum about 18 days after the explosion, although the brightest model reaches maximum somewhat later.

We used our Monte Carlo spectrum synthesis code (Mazzali & Lucy 1993, Lucy 1999, Mazzali 2000) to compute synthetic spectra for the three models. The code requires as

input a hydrodynamical model of the explosion and values for the luminosity L and the photospheric velocity v_{ph} at an epoch t . We can take both L and v_{ph} from the light curve calculations. However, such calculations are known to give a poor representation of the photospheric velocity, in particular at times past maximum (Fig. 3). At those epochs codes overestimate the velocities, most likely because the approximation of a gray photosphere is not valid at all wavelengths (Khokhlov et al. 1993, Höflich et al. 1995, Iwamoto et al. 2000, Mazzali, Iwamoto & Nomoto 2000). Therefore, we can use v_{ph} values from the light curve calculations to compute synthetic spectra at maximum, but we have to rely on velocity information from observed spectra to compute spectra at 15 days after maximum. We also computed spectra at one week before maximum, for completeness, using both L and v_{ph} from the light curve calculations. For each synthetic spectrum calculation, we used a ratio of Fe-group v. IME obtained by mixing the compositions of the layers above the photosphere in the particular explosion model. The relative abundances of the IME’s are based on the explosion model W7, and for the Fe-group the decay of ^{56}Ni into ^{56}Co and ^{56}Fe was taken into account. Stable Fe-group elements are buried deep in the ejecta, and they do not influence the spectra.

The integrated photometry from the synthetic spectra was used to compute $\Delta m_B(15)$. We obtained $\Delta m_B(15)$ values ranging from 1.1 to 1.5 mag. These values are comparable to those of observed spectroscopically normal SNe Ia. The numbers for the three models are given in Table 2.

Finally, we compare our synthetic spectra for the epochs -7 days, maximum and $+15$ days with the spectra of the same SNe used in Figure 2 for the light curve comparison. We use spectra taken at epochs as close as possible to those of the models. Figure 4 shows the pre-maximum spectra, Figure 5 the spectra at maximum light and Figure 6 the spectra at 15 days after maximum. The observed spectra have been corrected for redshift but not for

reddening, which is however small. The values of $\Delta m_B(15)$ for the various SNe are given in the figures. No attempt was made to obtain detailed fits to the spectra. The synthetic spectra appear to resemble the observed ones. It is remarkable that spectra obtained from such different models are actually not very different. This is because at a given epoch the photosphere is located at lower velocities in models that produce less ^{56}Ni , at least after about day 10 (see Fig. 3), but since the luminosity is also lower in these models the effective temperatures in the three models are similar. This is consistent with the results of Nugent et al. (1995). Also, the abundances in the layers that form the spectra, especially at and before maximum, are not much affected by the deep layers, and so the spectra are relatively insensitive to the large differences in ^{56}Ni mass.

6. Conclusions

Using a set of light curves and spectra computed for three representative models we have shown that the differences in the observed properties of SNe Ia all having Chandrasekhar-mass progenitors but producing different amounts of ^{56}Ni reproduce the observed dispersion of properties of at least *spectroscopically normal* SNe Ia. Our calculation procedure is not fully self-consistent because the photospheric velocities obtained from the light curve calculations are not always reliable, especially after maximum, and we had to use estimates from observed spectra. Nevertheless, the results are encouraging. Calculations with a self-consistent code (e.g. Nugent et al. 1997) could give more reliable results.

The range of properties displayed by the models we have studied is sufficient to encompass the observed properties of *spectroscopically normal* SNe Ia. However, *peculiar* SNe Ia, such as SNe 1991T and 1991bg, seem to be well outside this range, especially from a spectroscopic point of view. For SN 1991T there is spectroscopic evidence that ^{56}Ni was present also in the outer part of the ejecta (Mazzali et al. 1995), which would seem to

require a different explosion model (e.g. Yamaoka et al. 1992). SN 1991bg, on the other hand, was so faint and its light evolution so fast that it may be difficult to explain it within the framework of Chandrasekhar-mass explosions. The fact that several SNe very similar to either SN 1991T or SN 1991bg have been observed but that there are essentially no examples of objects that might fill the gap in properties between these very extreme cases and the range of ‘normal’ SNe Ia may suggest that these may actually be individual subtypes. More observations of SNe Ia are necessary to address this issue.

Acknowledgements. It is a pleasure to thank Peter Höflich for useful discussions concerning the behaviour of the opacity. We are grateful to David Branch, the referee, for his remarks on an earlier version of this paper. This work has been supported in part by the Grant-in-Aid for Scientific Research (12640233, 12740122) and COE research (07CE2002) of the Japanese Ministry of Education, Science, Culture, and Sports in Japan.

REFERENCES

- Arnett, D., 1982, ApJ 253, 785
- Arnett, D., 1996, *Supernovae and Nucleosynthesis*, Princeton Univ. Press, Princeton
- Brachwitz, F., Dean, D.J., Hix, W.R., Iwamoto, K., Langanke, K., Martinez-Pinedo, G.,
Nomoto, K., Strayer, M.R., Thielemann, F.-K., Umeda, H. 2000, ApJ 536, 934
- Branch, D., 1998, ARAA 36, 17
- Cappellaro E., Mazzali P.A., Benetti S., et al. 1997, A&A 328, 203
- Contardo, G., Leibundgut, B., Vacca, W.D., 2000, A&A 359, 876
- Della Valle, M., Kissler-Patig, M., Danziger, I.J., Storm, J., 1998, MNRAS 299, 267
- Drenkhahn, G., Richtler, T., 1999 A&A 349, 877
- Filippenko, A.V., Richmond, M.W., Branch, D., et al., 1992, AJ 104, 1543
- Fisher, A., Branch, D., Höflich, P., Khokhlov, A.M., 1995, ApJ 447, L73
- Fisher, A., Branch, D., Hatano, K., Baron, E., 1999, MNRAS 304, 67
- Hamuy, M., Phillips, M.M., Maza, J., Suntzeff, N.B., Schommerr R.A., Aviles, R., 1995, AJ
109, 1
- Hamuy, M., Phillips, M.M., Schommerr R.A., Suntzeff, N.B., Maza, J., Aviles, R., 1996a,
AJ 112, 2391
- Hamuy, M., Phillips, M.M., Suntzeff, N.B., Schommerr R.A., Maza, J., Aviles, R., 1996b,
AJ 112, 2398
- Hillebrandt, W., Niemeyer, J., 2000, ARAA, in press

- Höflich, P., Khokhlov, A.M., Wheeler, J.C., 1995, ApJ 444, 831
- Höflich, P., Khokhlov, A.M., Wheeler, J.C., Phillips, M.M., Suntzeff, N.B., Hamuy, M.,
1996, ApJ 472, L81
- Höflich, P., Wheeler, J.C., Thielemann, F.-K., 1998, ApJ 495, 617
- Iwamoto, K., Brachwitz, F., Nomoto, K., et al., 1999, ApJS 125, 439
- Iwamoto, K., Nakamura, T., Nomoto, K., et al., 2000, ApJ 534, 660
- Khokhlov, A., Müller, E., Höflich, P. 1993, A&A 270, 223
- Lucy, L.B. 1999, A&A, 345, 211
- Mazzali, P.A., 2000, A&A, in press
- Mazzali, P.A., Cappellaro, E., Danziger, I.J., Turatto, M, Benetti, S. 1998, ApJ 499, L49
- Mazzali, P.A., Danziger, I.J., Turatto, M., 1995, A&A 297, 509
- Mazzali, P.A., Iwamoto, K., Nomoto, K., 2000, ApJ, in press
- Mazzali, P.A. & Lucy, L.B. 1993, A&A 279, 447
- Nomoto, K., Thielemann, F.-K., Yokoi, K., 1984, ApJ 286, 644
- Nomoto, K., Yamaoka, H., Shigeyama, T., Kumagai, S, Tsujimoto, T., 1994, in Supernovae,
eds. S.A.Bludman et al., Amsterdam, Elsevier Science, 199
- Nugent, P., Phillips, M., Baron, E., Branch, D., Hautschild, P.H. 1995, ApJ 455, L147
- Nugent, P., Baron, E., Branch, D., Fisher, A., Hautschild, P.H. 1997, ApJ 485, 812
- Pauldrach A.W.A., Duschinger M., Mazzali P.A., et al. 1996, A&A 312, 525

- Phillips, M.M., 1993, ApJ 413, L105
- Pinto, P.A., & Eastman, R.G., 2000, ApJ 530, 757
- Pskovskii, Y.P., 1977, Sov. Astron. 21, 675
- Riess, A.G., Press, W.H., Kirshner, R.P., 1995, ApJ 438, L17
- Riess, A.G., et al, 1998, AJ 116, 1009
- Riess, A.G., et al, 1999, AJ 118, 2675
- Saha, A., Sandage, A., Labhardt, L., Tammann, G.A., Macchetto, F.D., Panagia, N., 1997, ApJ 486, 1
- Spyromilio, J., Meikle, W.S.P., Allen, D.A., Graham, J.R., 1992, MNRAS 258, 53P
- Suntzeff, N., 1996, in Supernovae and Supernova Remnants, eds. R.McCray, Z. Wang, Cambridge, Cambridge Univ. Press, 41
- Umeda, H., Nomoto, K., Kobayashi, C., Hachisu, I., Kato, M., 1999, ApJ 522, L43
- Woosley, S.E., & Weaver, T.E., 1994, in Supernovae, eds. S.A.Bludman et al., Elsevier Science, Amsterdam, 63
- Yamaoka, H., Nomoto, K., Shigeyama, T., Thielemann, F.K., 1992, ApJ 393, L55

Table 1. Parameters of the synthetic light curves

model (M_{\odot})	^{56}Ni mass (d)	$t(\text{max})$ (mag)	$M(\text{max})(\text{Bol})$ (mag)	$M(+15)(\text{Bol})$ (mag)	$\Delta m_{15}(\text{Bol})$
Ni04	0.4	18.0	-18.91	-17.82	1.09
Ni06	0.6	18.0	-19.14	-18.17	0.97
Ni08	0.8	18.5	-19.32	-18.37	0.95

Table 2. Parameters of the synthetic spectra

model	$M(\text{max})(B)$ (mag)	$B - V(\text{max})$ (mag)	$M(+15)(B)$ (mag)	$B - V(+15)$ (mag)	$\Delta m_{15}(B)$ (mag)
Ni04	-18.85	0.03	-17.39	0.85	1.46
Ni06	-19.04	0.03	-17.76	0.77	1.28
Ni08	-19.21	0.07	-18.13	0.56	1.08

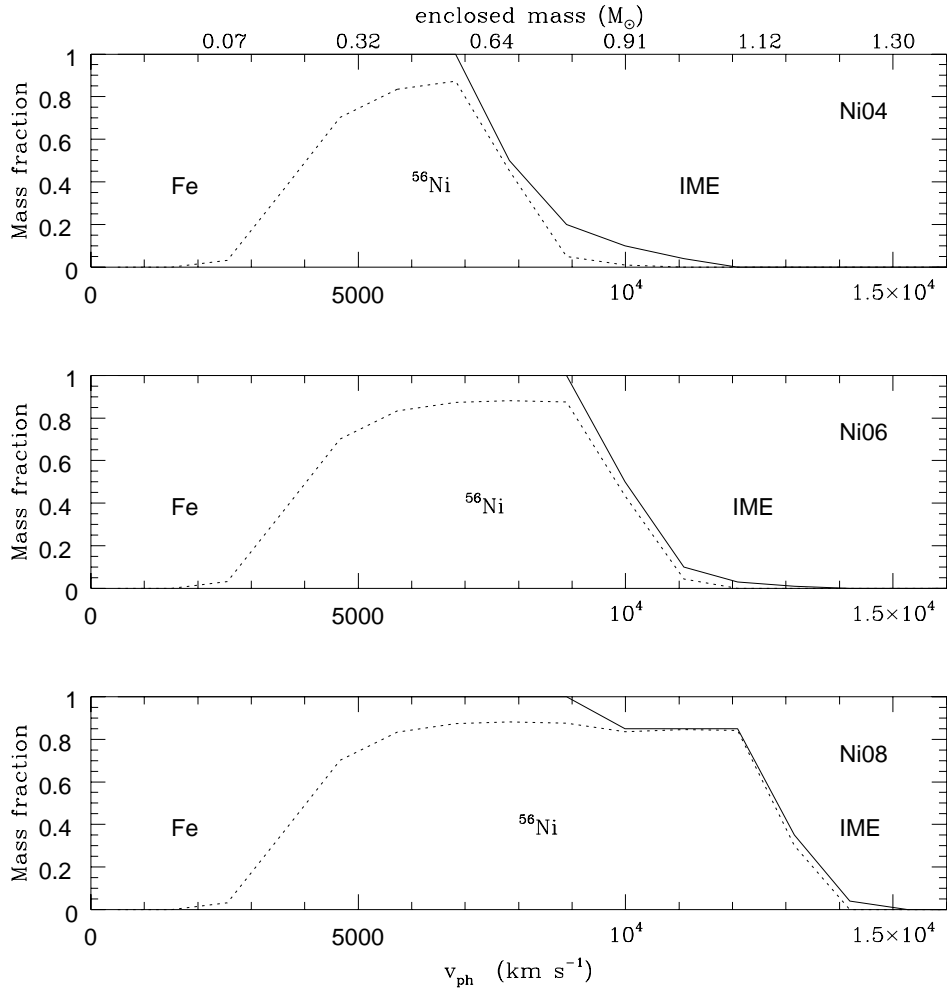


Fig. 1.— Composition of the three models.

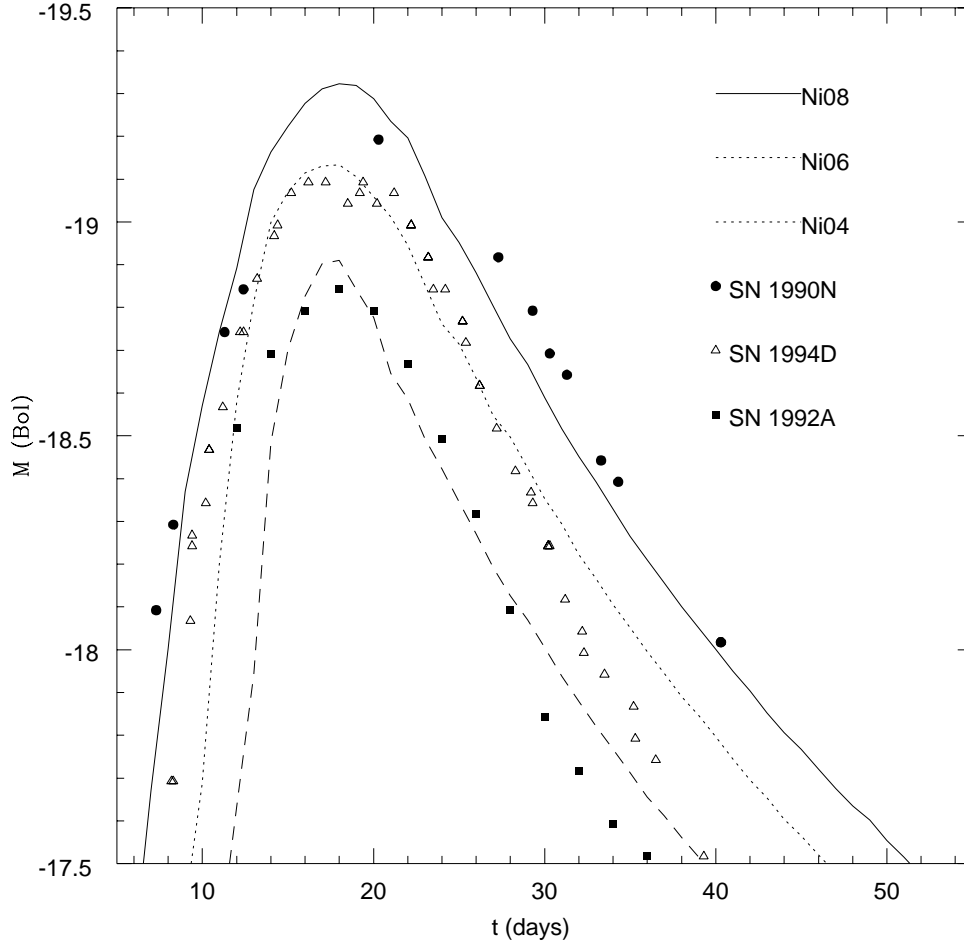


Fig. 2.— Synthetic bolometric light curves compared to *uvoir* light curves of spectroscopically normal SNe Ia.

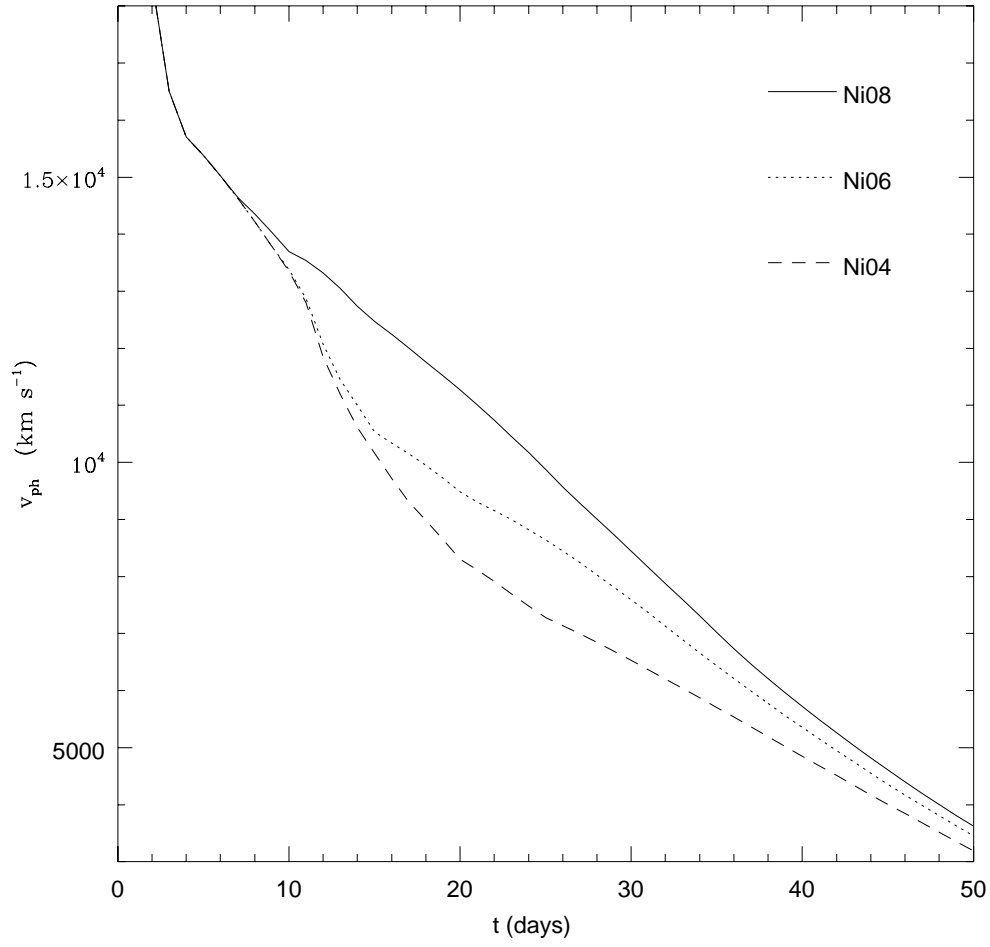


Fig. 3.— Photospheric velocities from the light curve calculations.

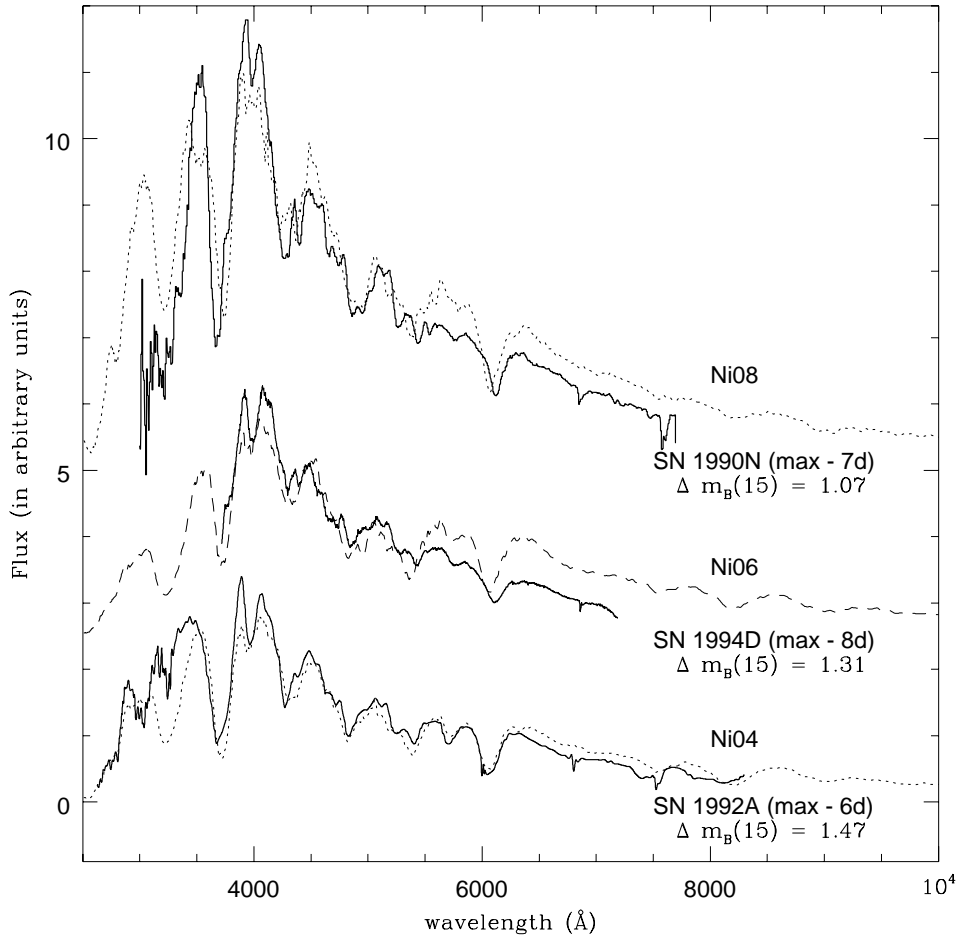


Fig. 4.— Synthetic and observed spectra at $t = Max - 7$ days.

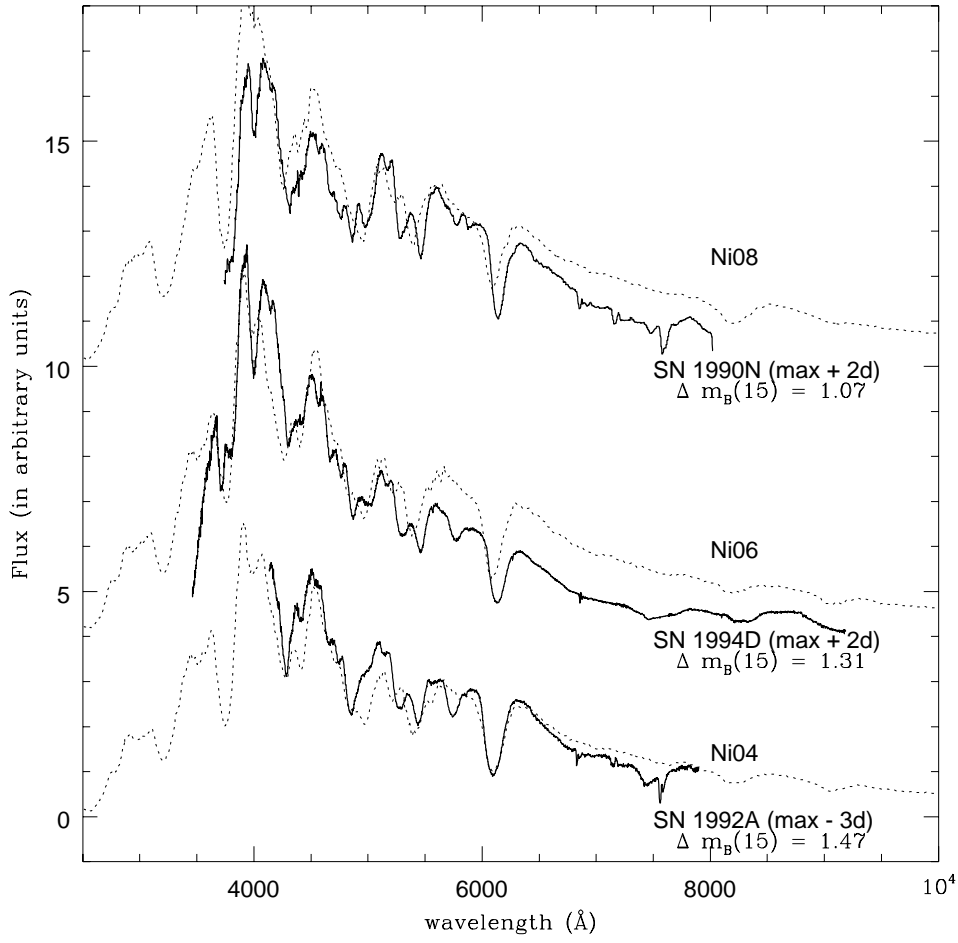


Fig. 5.— Synthetic and observed spectra at maximum.

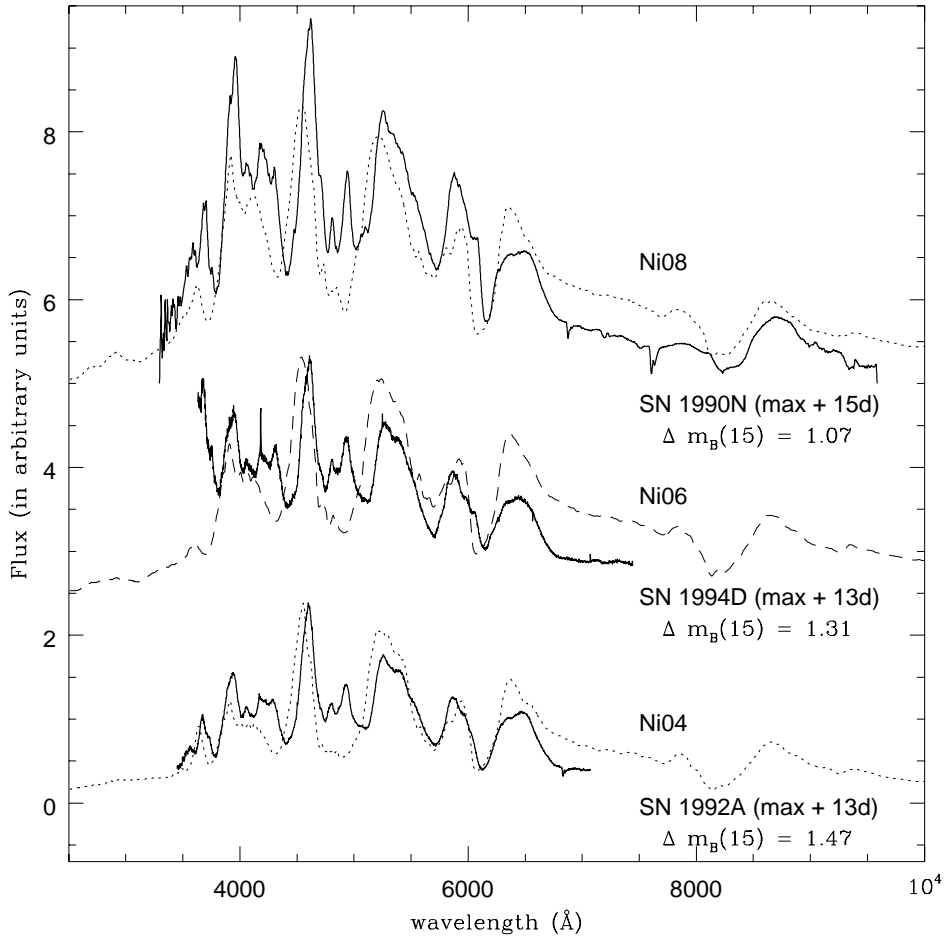


Fig. 6.— Synthetic and observed spectra at $t = Max + 15$ days.